Journal of Materials Chemistry B

Accepted Manuscript

ROYAL SOCIETY OF CHEMISTRY

www.rsc.org/materialsB

Journal of Materials Chemistry B

ARTICLE

Nanosheets-pores topographical titanium substrate: a biophysical regulator of mesenchymal stem cells fate

Kui Xu, Xinkun Shen, Weizhen Chen, Caiyun Mu, Chao Jiang, Yongchun Zhao, Kaiyong Cai*

Received 00th January 20xx,
Accepted 00th January 20xx

DOI: 10.1039/x0xx00000x

www.rsc.org/

Recent reports have demonstrated that nano- or microscale topography could enhance cellular functions of stem cells. In this study, a sub-micrometer topography composed of nanosheets-pores structures was fabricated on pure titanium surface by a simple vapor alkaline-treatment method to understand sub-micrometer topography mediating stem cell behaviors more profoundly. The topography were characterized by scanning electron microscopy, atomic force microscopy, X-ray photoelectron spectroscopy, X-ray diffraction and contact angle measurements, respectively. It specifically mediated cellular functions of rat bone marrow-derived mesenchymal stem cells (MSCs) on cellular and molecular levels under either normal medium or osteoinductive medium conditions. The experimental results indicated that the topography dramatically promoted the adhesion of MSCs grown onto the surface, but the shape, morphology and spreading of cells were not significantly affected. In addition, the study demonstrated that the formation of focal adhesion complexes (FAs) were highly dependent on the topography, which in turn affecting the subsequent biological functions of MSCs, especially accelerating osteogenic differentiation of MSCs under different conditions. Overall, the sub-micrometer topographical titanium substrate was an excellent biophysical regulator of mesenchymal stem cells fate, specifically inducing them to differentiate into osteoblasts.

Introduction

Stem cells play essentially important roles in regenerative medicine and tissue engineering,[1,2] due to their high proliferation, self-renewal capacity and potential differentiation into various non-self-renewable committed progenitors.[3,4] Their fates are highly directed by stem cell niches made up of diverse microenvironmental signals which could be roughly divided into two categories: physical signals and biochemical signals.[5] The biochemical signals include extracellular matrix component, soluble growth factors[6] *etc.*, while the biophysical signals include topography,[7] geometry,[8] elastic modulus[9] and dimension[10] of a substrate. These two kinds of signals in particular of the latter one mainly affect cell functions by interacting with receptors on stem cells membranes, resulting in the activation of intracellular cascade signaling in cellular events.

Recently, regulating the fates of stem cells with elaborate designed topography of a biomaterial attracted more and more attention in the related field. It has been demonstrated that nanometer-scale topographies, such as nanotubes,[10,11] nanorods,[12] nanoribbons,[13] nanogrooves[14] and nanopores[15] *etc.*, could positively affect the proliferation and osteogenic differentiation of mesenchymal stem cells (MSCs). For instance, Oh *et al.* confirmed that the adhesion, growth and differentiation of MSCs were intensely concerned with the dimensions of TiO_2 nanotubes nanotubes in a relatively small window.[10] Das *et al.* reported that helical nanoribbons with a specific periodicity of about 60 nm induced higher cell adhesion via the formation of focal adhesion complexes (FAs) and stronger cells commitment differentiating into osteoblasts than those of twisted nanoribbons with a periodicity of approximately 100 nm.[13] Thus, it is clear that a slight change in topography of a biomaterial would strongly affect the fates of MSCs. However, few studies have investigated with respect to the influence of sub-micrometer topographical surfaces with nanosheets- pores features on the proliferation and differentiation of MSCs. A previous *in vivo* study demonstrated that sub-micrometer grooved (300 nm (1:3)) titanium implants had significantly high bone-to-implant contact after implantation for 4 weeks,[16] which implying the intense influence of sub-micrometer topography on stem cells differentiation.

Commercially pure titanium (Ti) and its alloys, possessing good mechanical properties and bioinert properties, have been widely used in biomedical fields, such as orthopedic and dental surgery.[17,18] Whether *in vitro* or *in vivo* environments, a pure Ti material lacks desirable bioactive property since a smooth and dense passivation layer on its surface hinders the chemical bonding to bone.[19] Structurally, nature bone has distinct structures with dimensions from nano-, micro-, to macrometer, composing of

Key Laboratory of Biorheological Science and Technology, Ministry of Education, College of Bioengineering, Chongqing University, Chongqing 400044, PR China. E-mail: kaiyong_cai@cqu.edu.cn; Tel: +86-23-65102507

organic extracellular matrix (ECM) components and inorganic components.[20] Recent reports demonstrated that the formation and maturation of FAs were affected by the topographies of substrates, and then in turn regulating the biological functions of MSCs, especially adhesion and differentiation.[21,22] Thus, to exploit an approach for the fabrication of the topography of titanium substrates that closely mimicking the nano- or microscale architectures of nature bone is the inherent rationale for mediating the interactions between Ti implant and bone formation cells (osteoblasts, MSCs, *etc.*).

In this study, we report an approach for the fabrication of the sub-micrometer nanosheets-pores topographical titanium substrates. It was a simple alkaline treatment with sodium hydroxide, followed by ion exchange treatment and calcination treatment, thus generating sub-micrometer nanosheets-pores topography on Ti substrates to mimic natural bone architecture. We hypothesized that the sub-micrometer nanosheets-pores topographical Ti substrates with optimal scale could enhance the adhesion and osteogenic differentiation of MSCs. The potential mechanism was revealed by both qualitative and quantitative investigations of protein adsorption, cell adhesion, cell differentiation and the expressions of bone formation related mRNA/proteins (Runx2, Osterix, *etc.*), respectively.

Experimental section

Materials

Native titanium (Ti) disks (diameter: 15 mm; thickness: 3 mm) were provided by Northwest Institute for Nonferrous Metal Research, China. Bovine serum albumin (BSA), Fluorescein diacetate (FDA), Hoechst 33258, Dexamethasone, L-ascorbic acid, β-glycerophosphate, paraformaldehyde and Triton X-100 were provided by Sigma Aldrich Co. (St. Louis, MO, USA). Rhodamine-phalloidin was bought from Invitrogen Co. (USA). Anti-vinculin antibody was purchased from Santa Cruz Biotechnology Co. (USA). Alizarin red S sodium salt was provided by Alfa Aesar Co. (Tianjin, China). 3-(4, 5-dimethyl thiazol-2-yl)-2, 5-diphenyl tetrazolium bromide (MTT), p-nitrophenyl phosphate assay kit, bicinchoninic acid (BCA) assay kit, the mammalian protein extraction kit, peroxidase-conjugated goat anti-rabbit antibody and BCIP/NBT alkaline phosphatase staining kit were obtained from Beyotime Biotechnology Co. (Jiangsu, China). Phosphate buffer solution (PBS) was provided by Dingguo Biotechnology Co. (Beijing, China). Mouse anti-goat fluorescein isothiocyanate (FITC)-conjugated secondary antibody was supplied by ZSGB-BIO Co. (China). The specific primary antibodies (anti-β-actin, anti-Runx2, anti-Col I and anti-OPN) used in western blot were provided by Boster Co. (Wuhan, China). Other chemicals were purchased from Oriental Chemical Co. (Chongqing, China).

Samples preparation

TiO_2 nanosheets were prepared according to a previous study.[23] Ti disks were first polished with diamond pastes (No. 400-4000) and then sequentially rinsed with detergent, acetone, ethanol, and distilled water each for 20 min under sonication, respectively. The treated samples were dried at 60 °C for 24 h. Next, a sodium hydroxide (NaOH) solid layer was coated onto the Ti disks by steep lifting the Ti disks from NaOH/ ethanol solution (0.5 M) at a speed of 2 mm s^{-1} and dried in an oven at 60 °C for 30 min. Ti disks were divided into 3 groups corresponding to the different layers of NaOH solid (1, 2 and 3 layers, respectively). A teflon holder was used to horizontally hold the Ti disk being exposed above distilled water (5 mL) in a teflon lining. The distance between Ti disk and the water surface was about 3 cm. The teflon lining was sealed in a stainless autoclave and heated in an oven to 150 °C at a heating rate of 2 °C/min. The three kinds of Ti disks were treated for 3, 10 and 24 h against 1, 2 and 3 layers of NaOH solid coated samples, respectively. The above process was denoted as NaOH-treatment. Next, the treated Ti disks were gently rinsed with distilled water for 3 times and then immersed into 0.1 M hydrochloric acid (HCl) solution at 40 °C with shaking (120 strokes min^{-1}) for 2 h.[24,25] We named this process as HCl-treatment. Subsequently, the treated disks were rinsed with distilled water for 3 times and calcined in a muffle furnace at 450 °C for 2 h.[26,27] This process was marked as heat-treatment. In this way, we got three kinds of Ti substrates with

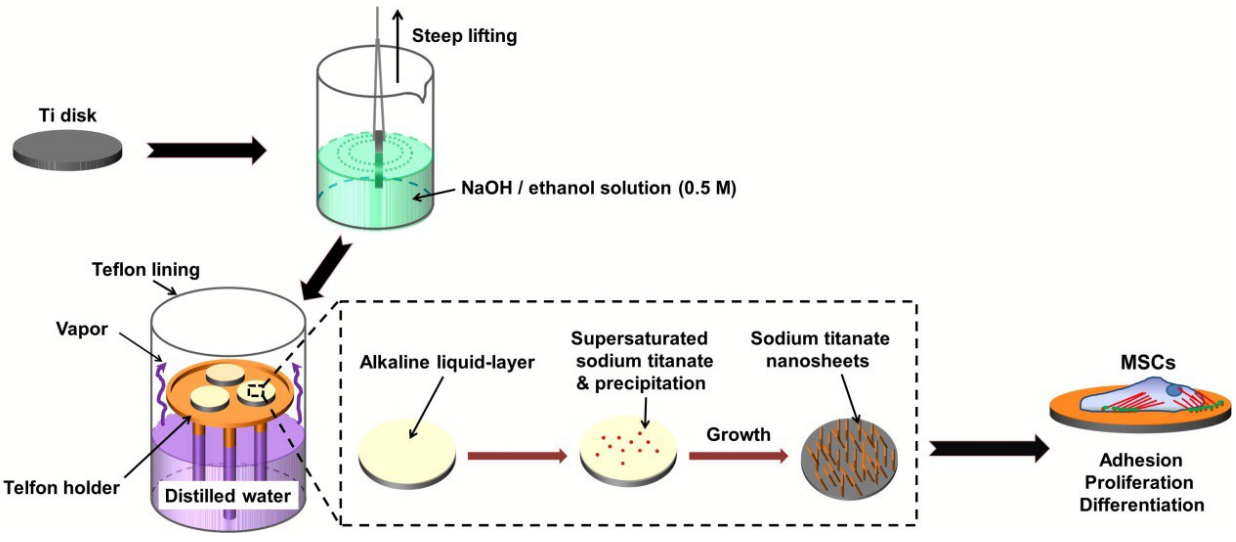

Fig. 1 Illustration of the fabrication of sub-micrometer nanosheets-pores structures on pure titanium surface and its biological responses.

TiO_2 nanosheets were denoted as S-TNSs, whereas the samples with medium length of TiO_2 nanosheets and long length of TiO_2 nanosheets were denoted as M-TNSs and L-TNSs, respectively. In the same way, we denoted pure titanium disk as Ti (control). All Ti samples were sequentially cleaned with acetone, ethanol, and distilled water each for 5 min under ultrasonication, respectively. The samples were sterilized in an autoclave under 0.1MPa at 120 °C for 30 min for *in vitro* experiments.

Surface characterization

The surface morphologies of all substrates were observed by field-emission scanning electron microscopy (SEM, FEINova 400 Nano SEM, Phillips, Holland) and atomic force microscopy (AFM, Dimension, Bruker, Germany). The chemical compositions of the substrates were determined by X-ray photoelectron spectroscopy (XPS) using the model PHI 5600 system (Perkin-Elmer) with an Mg Kr source (1253.6 eV). The crystalline phases of the samples were characterized by X-ray diffraction (XRD, D/Max 2500PC, Rigaku, Japan). Contact angles of the substrates were measured by a model 200 video-based optical system (Future Scientific Co., Tai Wan, China) according to an our previous study.[27]

Cell culture

MSCs were isolated from bone marrow of rats' femur and tibia (SD rat, with weight of about 150 g).[28] Cells were cultured with normal medium (NM), i.e., DMEM (low glucose) supplementing with 10% fetal bovine serum (FBS, Gibco) at 37 °C under 5% CO_2 atmosphere. Cell media was changed every 12 hours in the first 48 hours, and then every 2 days. After confluence, cells were detached with 0.25% (w/v) trypsin in 0.01% (w/v) $EDTANa_2$/ PBS solution, centrifuged, and re-suspended in the new complete medium. Osteoinductive medium (OM) was prepared by adding 100 nM dexamethasone, 50 mg/ml L-ascorbic acid, and 10 mM β-glycerophosphate to the NM.[29-31] We used MSCs at the 3rd passage for experiments. To induce osteogenic differentiation, cells were seeded and cultured onto the substrates with the NM for the first day and with the OM for the next incubation period.

Protein content assay

The total intracellular protein content assay was performed according to a previous study,[32] and the amounts of absorbed protein onto the surfaces of substrates were quantified in accordance with another study.[33] In the former case, MSCs were cultured onto different Ti substrates and tissue culture polystyrene (TCPS) at an initial cell seeding density of 1×10^4 cells/cm^2 (24-well plate) for 7 and 14 days, respectively. Cells were then lysed by 1% Triton X-100/ PBS solution. In the latter case, 200 µL of bovine serum albumin (BSA) solution (1 mg/mL protein/ PBS) was pipetted onto each Ti substrate and TCPS (control) in a 24-well cell culture plate. Then, the plate was placed in a sterile humidified incubator at 37 °C for 2 and 4 h, respectively. After that, the non-adherent proteins were removed and each well was washed with PBS for 3 times. Then, 200 µL of sodium dodecyl sulfate solution (SDS, 2%) was added into each well and the plates were subsequently incubated at 37 °C overnight to extract the adhered proteins. To determine either the total intracellular protein content of cells or the absorbed protein content onto the surfaces of different Ti substrates, BCA assay was performed, which was based on Lowery technique.[34] The absorbance was measured at a wavelength of 570 nm with a spectrophotometric microplate reader (Bio-Rad 680). The protein content (expressed as mg) was determined from a standard absorbance curve versus known concentration of albumin run in the parallel experiment.

MTT assay and FDA staining

According to a previous study,[35] MTT assay was used to evaluate proliferation of MSCs cultured onto different Ti substrates (n=5). Briefly, cells were cultured onto different Ti substrates and TCPS at an initial density of 1×10^4 cells/cm^2 for 7 and 14 days, respectively. Next, cell media was changed into serum-free media and 100 µL of MTT (5 mg/mL) was added to each well. Subsequently, the cell culture plates were incubated at 37 °C for another 4 h. After removing the MTT-containing medium, 0.8 mL of dimethyl sulfoxide (DMSO) was added to each well to dissolve formazan crystal. Finally, the optical absorbance of the solution was measured at 490 nm with a spectrophotometric microplate reader (Bio-Rad 680).

Fluorescein diacetate (FDA) staining was performed according to a previous study.[36] MSCs were seeded onto different substrates in 24-well plate and TCPS for 1, 4 and 7 days. Then, FDA solution (5 mg/ml, FDA/acetone) was dropped into the cell wells (3 µL/well). After incubation at 37 °C for 20 min, the samples were visualized by a fluorescence microscopy with excitation at 488 nm.

Cell morphology

Cells were cultured onto different Ti substrates at an initial density of 4×10^3 cells/cm^2 for 2 days. The samples were then rinsed with PBS twice and fixed with 4% paraformaldehyde. Before SEM examination, the samples were dehydrated with gradient ethanol solutions (20, 40, 60, 80, 90, 95 and 100 v/v%) each for 15 min. After that, the replacement processing was performed with tert-butyl alcohol for 30 min. Finally, the samples with cells were coated with gold for SEM observation, which was performed at 5 kV.

Immunofluorescence of vinculin, actin and cell nucleus

Cells seeding procedure was the same as above. After incubation for 2 days, the cells grown onto each substrate were fixed with 4% paraformaldehyde at 4 °C for 30 min. Samples were then washed with PBS for 3 times and permeablized with 0.2% Triton X-100/ PBS solution at room temperature for 2 min. Next, the treated samples were washed with PBS for 3 times and incubated with 1% BSA/ PBS solution at 37 °C for 1 h. Subsequently, goat monoclonal antibody against vinculin (1:400) was added at 4 °C overnight.[37] After that, mouse-antigoat fluorescein isothiocyanate (FITC)-conjugated secondary antibody (1:200) was added at 37 °C for another 1 h.[37] The samples were rinsed with PBS for 3 times. Finally, the treated samples were stained with 5 U/mL rhodamine-phalloidin (Invitrogen) at 4 °C overnight and counterstained with 10 µg/mL Hoechst 33258 at room temperature for 5 min.[37] The stained samples were mounted with 90% glycerinum and observed with CLSM (TCS SP5, Leica, Germany).

According to a previous study,[22] to understand the effect of topological structure for FAs of MSCs adhered to different Ti substrates, we quantified the vinculin (an important component of FAs, Fig. 6 E) expression of MSCs by the area and fluorescence intensity analysis of vinculins to indirectly observe the formation of FAs. The quantitative data of each group was obtained from two experiments with 3 samples in each experiment, and the fluorescence images of 60 cells in each group were selected to be analyzed by Image Pro Plus 6.0 (IPP 6.0).

Alkaline phosphatase (ALP) staining and intracellular ALP activity assay

The ALP staining and activity assay were performed according to previous studies.[38,39] Cells were seeded onto different Ti substrates at an initial density of 1×10^4 cells/cm^2. After culturing for 4 and 7 days, the samples were washed and fixed as above. The ALP staining was performed with BCIP/NBT alkaline phosphatase staining kit for 15 min. After rinsing with distilled water for 3 times, the stained samples were observed by a stereoscopic microscope (MVX10, Olympus).

For intracellular ALP activity assay, cells were lysed by 1% Triton X-100/ PBS solution with three freeze-thaw cycles. Following the centrifugation of the lysates, the total intracellular protein and ALP activity were determined with BCA kit and p-nitrophenyl phosphate assay kit, respectively. The ALP activity (expressed as μmol of converted p-nitro-phenol/min) was normalized by the total intracellular protein production. The ALP activity was thus expressed as μmol p-nitrophenol/min/mg protein.

Alizarin Red Staining and determination of calcium content

In this study, cells were seeded onto different Ti substrates and TCPS at an initial density of 1×10^4 cells/cm^2. After culture for 21 days, cells were stained by Alizarin Red Staining (ARS) according to a previous study.[40] Briefly, cells were fixed with 4% paraformaldehyde at 4 °C for 30 min and stained with Alizarin Red (40 mM, pH=4.1) at room temperature for another 20 min. After washing with distilled water for 3 times, acetic acid (10% v/v) solution was added to each well. Subsequently, the samples were incubated at 37 °C for 30 min. Finally, the samples were rinsed thrice with distilled water and observed by a stereoscopic microscope (MVX10, Olympus).

To determine calcium content, cells were scraped from the sample surface and repeatedly flushed with the bulk solution. Then, the solution was transferred into a vial and vortexed for 30 s. After heating at 85 °C for 10 min and centrifuged for 15 min, the supernatant was transferred into a new vial, and 10% ammonium hydroxide (NH_4OH) was added to neutralize the acid. The absorbance of the solution was measured with a microplate reader (Bio-Rad 680) at a wavelength of 405 nm.

Quantitative real-time polymerase chain reaction (qRT-PCR)

MSCs were cultured on different Ti substrates at an initial density of 2×10^4 cells per well of a 24-well plate. After culture for 14 days, the total RNA was extracted using RNA extract kit (Bioteck Co.) according to the manufacturer's instructions. First-stranded cDNA was synthesized with a commercially available kit (Takara, China). Real-time PCR was performed with a Bio-Rad CFX manager system. Amplification was performed with two-step cycling condition at 98 °C for 3 min, followed by 45 cycles at 98 °C for 2 s, 58 °C for 15s and 72 °C for 30 s. The selected specific primer sequences were listed in Table 1. Melting curves were recorded with continuous fluorescence data acquisition during the 65-95 °C melting process. Reactions were performed in triplicate. Data were analyzed with the Bio-Rad CFX Manager. Each qRT-PCR was performed in triplicate for qRT-PCR yield validation. The targeted gene expression was normalized to β-actin, which was used as a housekeeping gene.

Western blot

MSCs were seeded onto TCPS and different Ti substrates at an initial density of 1×10^4 cells/cm^2 in 6-well plates for 14 days. The total intracellular proteins were obtained according to the instruction of the mammalian protein extraction kit. The 10% sodium dodecyl sulfate (SDS)-polyacrylamide gel and 0.22 μm polyvinylidene difluoride membrane (PVDF, Pall, USA) were employed to separate and gather proteins. After blocking non-specific adsorption sites with 5% skimmed milk solution, the membranes were then incubated with specific primary antibodies (anti-β-actin, anti-Runx2, anti-Col Ⅰ and anti-OPN) at 4 °C overnight. The antibody-bound membranes were further treated with peroxidase-conjugated goat anti-rabbit antibody at ambient temperature for 1 h. Finally, the development process was performed with an enhanced ECL Western Blot Kit (Thermo, USA) using a luminescent imager (VersaDoc MP 4000 Bio-Rad, USA). Image analysis was performed with Quantity One (version 4.6.2).

Image and statistical analysis

Image Pro Plus 6.0 (IPP 6.0) and Adobe Photoshop CS4 11.0 (PS CS4 11.0) were employed to analyze nanosheets length and surface pore diameters. In order to calculate the normalized focal adhesion value and areas of cell, data from fluorescence images were analyzed by IPP 6.0. All data were expressed as means ± standard deviation (SD). The statistical analysis was performed with Origin Pro (version 7.5) via one-way analysis of variance (ANOVA) and Students's t-test. The confidence levels were set as 95% and 99%.

Results and discussion

Design and characterization of substrates

In this study, the sub-micrometer topography composed of nanosheets was generated on titanium substrates via combined NaOH-treatment, HCl-treatment and heat -treatment.[23, 24] A NaOH solid layer was pre-coated onto Ti substrates and sealed in a stainless autoclave for further treatment. When increasing the temperature, a thin alkaline liquid-layer would be rapidly developed on the surfaces of Ti substrates due to the wetting of the pre-coated NaOH solid by water vapor. Then, dissolution of Ti substrates by NaOH would occur to form sodium (Na) titanate at the surfaces of Ti substrates.[23] The titanate species were continuously produced at the interface of Ti substrates and liquid-

Table 1. Real-time PCR primers used in this study.

Target gene	*GeneBank (Accession no.)*	*Primers*	*Product size (bp)*
β-actin	NM_031144.2	GGAGATTACTGCCCTGGCTCCTA GACTCATCGTACTCCTGCTTGCTG	150
Runx2	NM_053470.2	GCCGTAGAGAGCAGGGAAGAC CTGGCTTGGATTAGGGAGTCAC	150
Osterix	NM_181374.2	CGGCAAGGCTTCGCATCTG GGAGCAGAGCAGACAGGTGAACT	166
ALP	NM_013059	AGCGACACGGACAAGAAGC GGCAAAGACCGCCACATC	183
Col I	NM_053304.1	CCTGAGCCAGCAGATTGA TCCGCTCTTCCAGTCAG	106
OPN	M99252	GACAGCAACGGGAAGACC CAGGCTGGCTTTGGAACT	216
OCN	M11777	GAGGGCAGTAAGGTGGTGAA CGTCCTGGAAGCCAATGTG	154

layer, and rapidly reached supersaturation state for precipitation, leading to structure formation and further growth. Admittedly, the NaOH-treatment readily inserted sodium into the surfaces of Ti substrates under this circumstance.[41] This titanate structure could be represented with $H_{0.7-x}Na_xTi_{1.825}\square_{0.175}O_4{\cdot}H_2O$ (where $\square$ =vacancy), which could be regarded as a ion exchange product of $H_{0.7}Ti_{1.825}\square_{0.175}O_4{\cdot}H_2O$.[23] Nevertheless, previous studies confirmed that the removal of Na in such structure was essentially important for achieving high *in vitro* osteoinductive ability and *in vivo* bioactivity.[24, 25, 42] To keep the desired topography while changing its chemical composition, the samples were further treated with 0.1M HCl solution. Thus, the Na in the structure was completely replaced by hydrogen (H), leading to the occurrence of $H_{0.7-x}Na_xTi_{1.825}\square_{0.175}O_4{\cdot}H_2O$ transforming into $H_{0.7}Ti_{1.825}\square_{0.175}O_4{\cdot}H_2O$. Subsequently, the samples were calcined at 450 °C for 2 h, resulting in the sheet-like titanate structure changed to TiO_2 nanosheets, which in turn affecting the biological functions of MSCs (adhesion, proliferation and differentiation etc.) (Fig. 1).

The morphologies of the fabricated Ti substrates were firstly characterized by SEM (Fig. 2 A). Pure Ti substrate displayed relatively smooth surface morphology (Fig. 2 A, a & a1). While the treated Ti substrates presented rough surface morphology. The vertically aligned nanosheets were uniformly formed onto the Ti surfaces (Fig. 2 A, b & b1, c & c1, d & d1). To reveal the depth of the

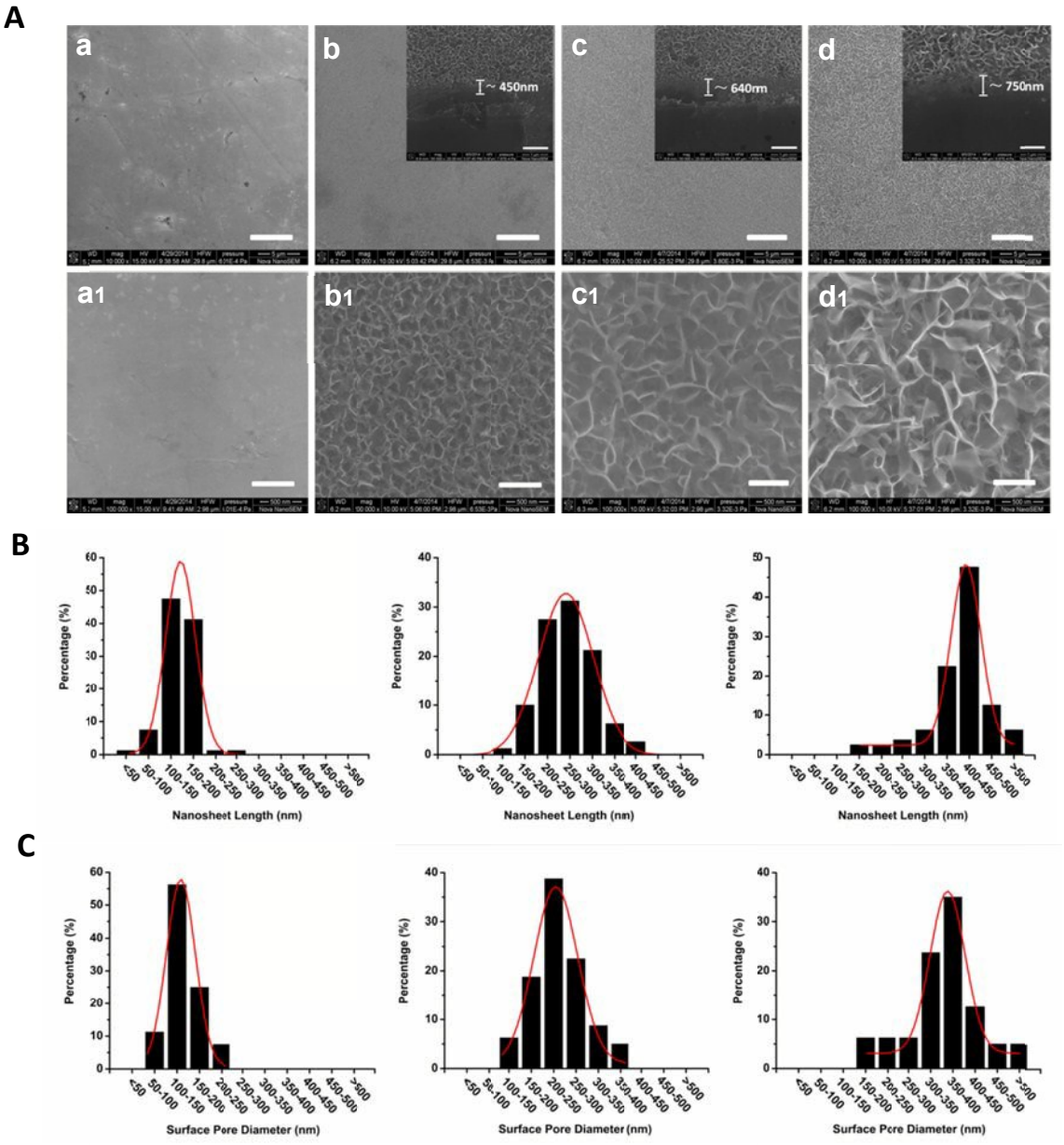

Fig. 2 (A) Representative SEM images of different substrates: Ti (a & a1), S-TNSs (b & b1), M-TNSs (c & c1), L-TNSs (d & d1) (scale bar, 5 μm for a, b, c and d, 500 nm for a1, b1, c1 and d1, respectively). Representative cross-sectional SEM images of S-TNSs, M-TNSs and L-TNSs were displayed at the top right corners of corresponding SEM images (b, c and d, respectively) (Scale bar, 1 μm); (B) Quantification of nanosheet lengths of different substrates: (a) S-TNSs, (b) M-TNSs, and (c) L-TNSs, respectively; (C) Quantitative surface pore diameters of different substrates: (a) S-TNSs, (b) M-TNSs, and (c) L-TNSs, respectively. Quantitative data of (B) and (C) were obtained by Image Pro Plus 6.0 (IPP 6.0) and Adobe Photoshop CS4 11.0 (PS CS4 11.0) (n=80).

formed TiO_2 layer on different Ti substrates, we conducted 45°-cross-sectional SEM studies on different samples. It was interesting to note that three regions presented on the surfaces of Ti substrates (inserted SEM images in Fig. 2 A, b, c, and d). The top region was filled with nanosheets, and the middle region was a corrosion region, while the bottom region was pure Ti. The depths of the above two layers for S-TNSs, M-TNSs and L-TNSs substrates were about 450, 640 and 750 nm, respectively.

A previous study proved that the average thickness of the nanosheets was about 10 nm, which was irrelevant with the reaction time.[23] However, the reaction time could significantly affect the length of the nanosheets. The histograms in Fig. 2 B show the length distributions of the nanosheets formed onto different Ti 100 - 200 nm (S-TNSs), 200 - 350 nm (M-TNSs) and 400 - 450 nm (L-TNSs), respectively. Furthermore, it could be observed that the adjacent 2 - 4 nanosheets formed into a pore. Fig. 2 C shows the diameter distribution of the pores on S-TNSs, M-TNSs and L-TNSs substrates, respectively. The average diameters of the pores were roughly 100 - 200 nm, 200 - 300 nm and 300 - 400 nm corresponding with those three kinds of substrates above, respectively.

Next, we employed AFM to both qualitatively and quantitatively characterized different Ti substrates. The surface morphology revealing by 3D images demonstrated similar tendency to that of SEM observation (Fig. 3 A, a vs b, c & d). Quantitative surface roughness analysis was also performed in this study (Fig. 3 B). The L-TNSs displayed a relatively rough morphology with an average roughness (Ra) of 0.044 ± 0.003 μm when compared with those of

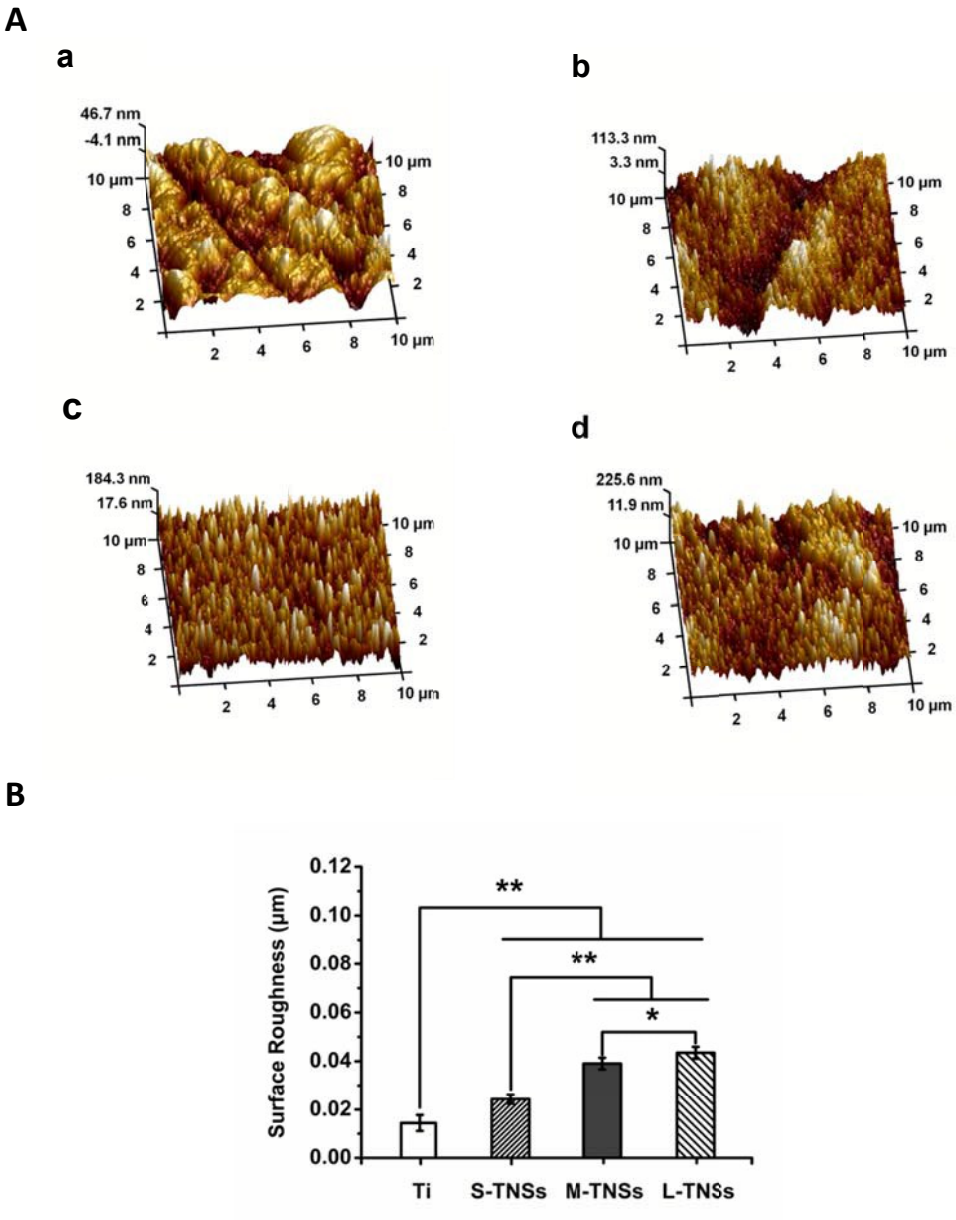

Fig. 3 (A) Representative AFM images of Ti (a), S-TNSs (b), M-TNSs (c) and L-TNSs (d); and (B) Surface roughness of Ti, S-TNSs, M-TNSs and L-TNSs substrates. Error bars represent means ± SD for n=4, *p<0.05, **p<0.01.

0.039 ± 0.003 μm, 0.024 ± 0.002 μm 0.015 ± 0.004 μm for M-TNSs, S-TNSs and Ti substrates, respectively. Distinctly, these structures presented sub-micrometer scale topography. Thus, we called it as sub-micrometer nanosheets-pores topography.

To investigate the surface chemistry of different Ti substrates, XPS characterization was performed. From the spectra of Ti (Fig. 4 A, a), S-TNSs (Fig. 4 A, b), M-TNSs (Fig. 4 A, c) and L-TNSs (Fig. 4 A, d), the feature peaks of titanium (Ti), carbon (C) and oxygen (O) could be observed. The peaks of carbon was attributed to surface contamination.[33] All samples displayed characteristic peaks of approximately 461.08 and 532.08 eV, which were assigned to Ti 2p3 and O1s, respectively. Compared with pure Ti substrate, S-TNSs, M-TNSs and L-TNSs substrates displayed relatively strong O1s signal, which indirectly suggests that Ti was mainly presented as a form of TiO2 at the outermost surfaces of these treated Ti substrates.[43] Furthermore, the characteristic peak of Na could not be found in any survey scan spectra, which suggests that the Na in the titanate nanosheets was completely replaced by hydrogen (H).

It had been shown that the anatase phase of Ti substrates has more hydroxyl groups and higher surface energy than the others crystalline phases, resulting in its preferable bioactivity.[44] This was the another reason to calcine the Ti substrates at 450 °C for 2 h. To reveal crystalline phases of different Ti substrates, X-ray diffraction (XRD) analysis was performed (Fig. 4 B). Pure Ti displayed characteristic peaks of α-Ti (No. 44-1294), such as (100), (002) and (102) peaks around 2θ=34.90°, 38.22° and 52.82°, respectively.[45,46] After NaOH-treatment, HCl-treatment and heat-treatment, additional peaks around 2θ=25.26°, 27.42°, 37.66°, 48.02°, 53.92°

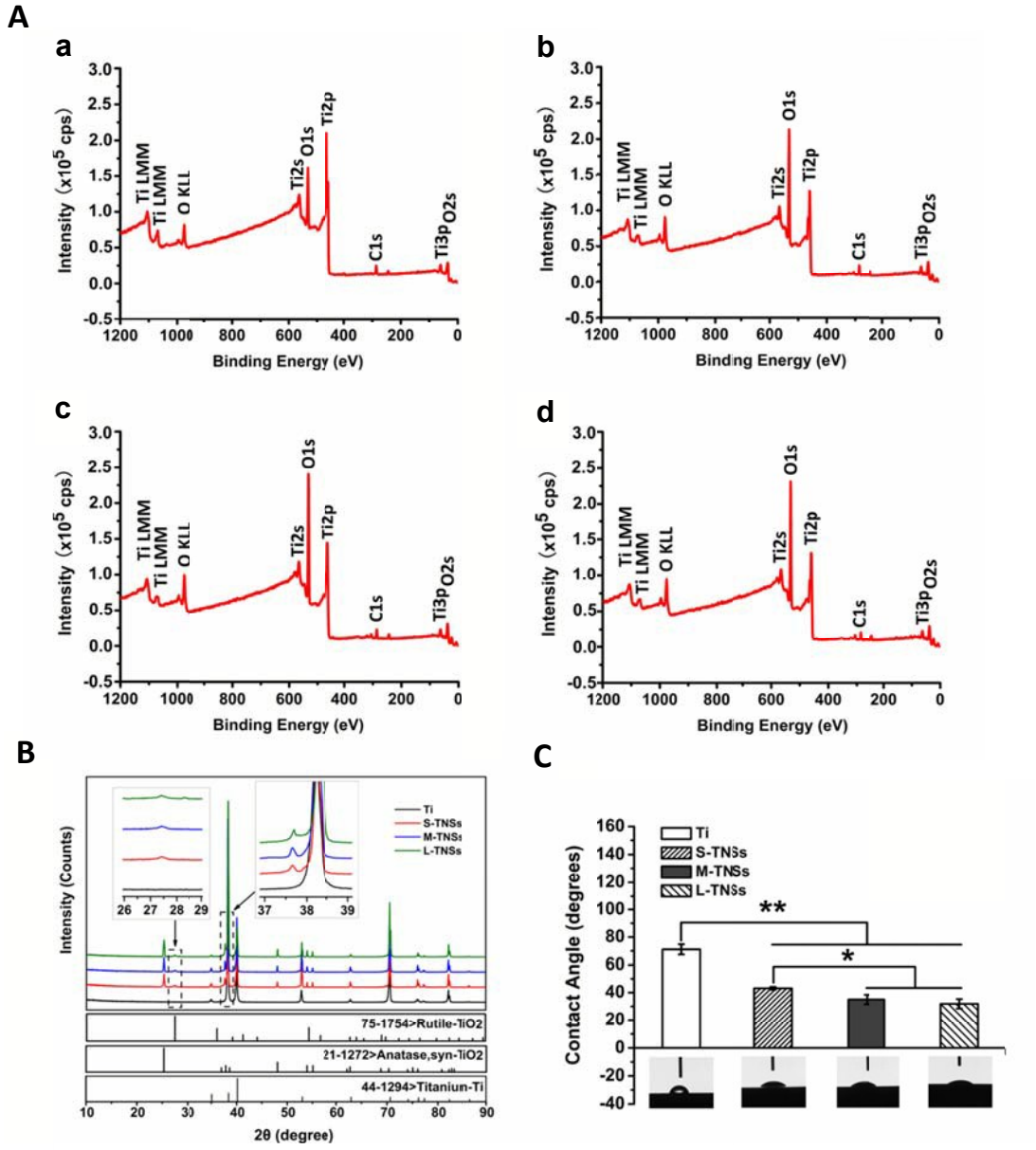

Fig. 4 Physical and chemical characteristics of different substrates: (A) XPS survey spectra of Ti (a), S-TNSs (b), M-TNSs (c) and L-TNSs (d); (B) XRD patterns of Ti, S-TNSs, M-TNSs and L-TNSs; and (C) Water contact angles of different Ti substrates. Error bars represent means ± SD for n=4, *p<0.05, **p<0.01.

and 55.02° were observed, which were attributed to anatase Ti (No. 21-1272) and rutile Ti (No. 75-1754).[47] These results demonstrated that $H_{0.7}Ti_{1.825}\square_{0.175}O_4{\cdot}H_2O$ was converted into a mixture of anatase and rutile TiO2 after heat-treatment. Moreover, it was easy to notice that the primary characteristic peaks of rutile Ti (2θ=27.42°) was very weak (Fig. 4 B), which was related to the low calcination temperature in this study. Thus, we obtained TiO_2 nanosheets structure through those treatments, mainly in anatase phase.

To evaluate the hydrophilic/hydrophobic property of different Ti substrates, we performed water contact angles measurements. As shown in Fig. 4 C, pure Ti substrates displayed contact angle of 71.1 ± 3.7°. In contrast, S-TNSs, M-TNSs and L-TNSs substrates displayed obvious hydrophilic properties with contact angles of 43.1 ± 1.0°, 35.0 ± 3.5° and 31.9 ± 3.4°, respectively. The significant difference ($p<0.01$) between pure Ti and other Ti substrates was contributed to factors as follows: (1) the increased surface hydroxyl contents; (2) the change of surface topography; and (3) the change of surface chemical compositions; whereas the significant differences ($p<0.05$) between S-TNSs and other Ti substrates was only attributed to the variation of surface topography. In addition, a previous study reported that the anatase nanosheets film showed superhydrophilicity with contact angle of around 10°; however, it was fabricated with aqueous urea solution and the nanosheets consisting of ammonium titanate ($(NH_4)_2Ti_xO_{2x+1}$).[48]

In a word, all titanium substrates shared similar surface chemistry, while having different surface topography with submicro-/nanostructures. Thus, these series of Ti substrates could be served as good model for the investigation of how sub-micrometer topography influence biological responses (protein adsorption, cell behaviors etc., especially the relationships between cells and topography), which is precisely a required in-depth research topic.

It is well known that, there are quite a lot of other surface modifications such as electrochemical oxidation (ECO),[10, 11] microarc oxidation (MAO)[49] *etc.* Nevertheless, as for MAO technique, the applied high voltage is not a security or economic choice. As for ECO technique, it is difficult to fabricate ideal sub-micrometer topography of a substrate. Apparently, comparing with these surface modification techniques, our simple method was easily to obtain desired sub-micrometer topography with controllable size and chemical composition, which lying down ground basis for the accurate control of the fates of MSCs grown onto the specific topographies.

Protein adsorption

Fig. 5 shows the albumin adsorption quantities on all titanium substrates and TCPS, which were determined by BCA assay. After incubation for 2 h, statistically significant difference of the adsorbed amount between Ti and L-TNSs ($p<0.05$) was observed. After incubation for 4 h, statistically significant differences in respect to protein adsorption amount were noticed between Ti and L-TNSs ($p<0.01$), Ti and M-TNSs ($p<0.05$), Ti and S-TNSs ($p<0.05$), L-TNSs and S-TNSs ($p<0.05$).

Protein adsorption onto a substrate (quantity, density, conformation, and orientation) highly depends on the chemical and physical characteristics of the substrate surface.[33, 50] As all Ti samples shared similar surface chemistry, the surface physical characteristics of the Ti samples dominantly affected on the protein

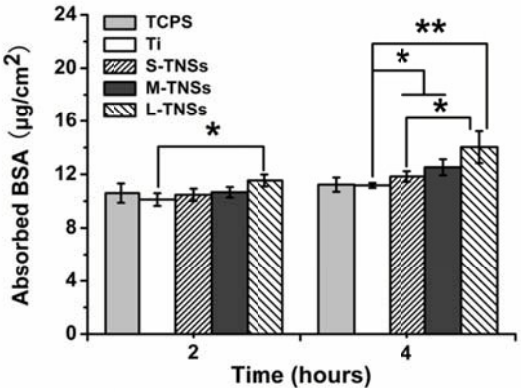

Fig. 5 Quantitative BSA adsorption onto different surfaces of Ti substrates. Each quantitative datum was obtained from two experiments with 3 samples in each experiment. Error bars represent means ± SD for n=6, *p<0.05, **p<0.01.

adsorption. In this study, both the lengths of nanosheets and diameters of pores were in sub-micrometer magnitude, which displayed significant influence on protein adsorption behaviors. Although a previous study confirmed that nanometer scale structure had little effects on the protein adsorption amount,[51] the nano scale features (*e.g.* nanosheets) may be helpful for retaining protein conformation/bioactvity, in turn positively affecting cells behaviors.[52]

Cell morphology

Cell adhesion is the crucial basis of the interaction between cells and a material, which in turn affecting cells proliferation and differentiation. To investigate cell adhesion behavior of MSCs, we characterized cell morphologies of MSCs cultured on different Ti substrates by SEM (Fig. 6 A) and CLSM via a triple staining of actin (cytoskeleton), vinculin and nuclei (Fig. 6 B). A similar cell spreading trend was observed on all Ti samples, which was also revealed by normalized ratio of cell overall areas to nuclei areas via image analysis (Fig. 6 C). The result suggests that all Ti substrates had good cytocompatibility. Nevertheless, the MSCs adhered to the treated Ti substrates displayed more noticeable filopodia extensions when comparing with those grown onto native Ti substrates (Fig. 6 A, arrows). The result indicates that the treated Ti substrates had great potential for improving cell adhesion.

FAs are complexes of multifarious proteins and lie at the convergence of integrins and actin filaments (F-actin; cytoskeleton).[53] Cells adjust FAs in response to changes regarding biochemicals, topographical structures, and physical forces presenting in their ECM environment.[53, 54] Normally, cell adhesion is mediated by transmembrane integrin protein. Vinculin is an intracellular protein, and also is an important component of FAs, playing a crucial role in initial cell adhesion and cytoskeletal development.[10] Vinculin expression indicates the FAs formation and maturation. As shown in Fig. 6 B, MSCs grown onto the treated Ti substrates displayed higher vinculin expression than those of native Ti substrates. Next, we quantified the vinculin expression of MSCs adhered to different Ti substrates by the area and fluorescence intensity analysis of vinculins. The normalized vinculin areas of cells (Fig. 6 D) increased in an order of Ti＜S-TNSs＜M-TNSs＜L-TNSs.

While a similar tendency for the normalized mean fluorescence intensity per cell of vinculin was observed (Fig. 6 E).

The potential mechanism of surface topography-induced cell focal adhesions formation and maturation was proposed as follows (Fig. 6 F): with increasing the sizes of nanosheets, the larger-sized nanosheets exert more intense stimulation to the integrins, a kind of transmembrane proteins associated with cell adhesion and differentiation of MSCs, which accelerates the FAs formation. The above results clearly demonstrated the stimulation of sub-micrometer topography on the adhesion of MSCs. The longer

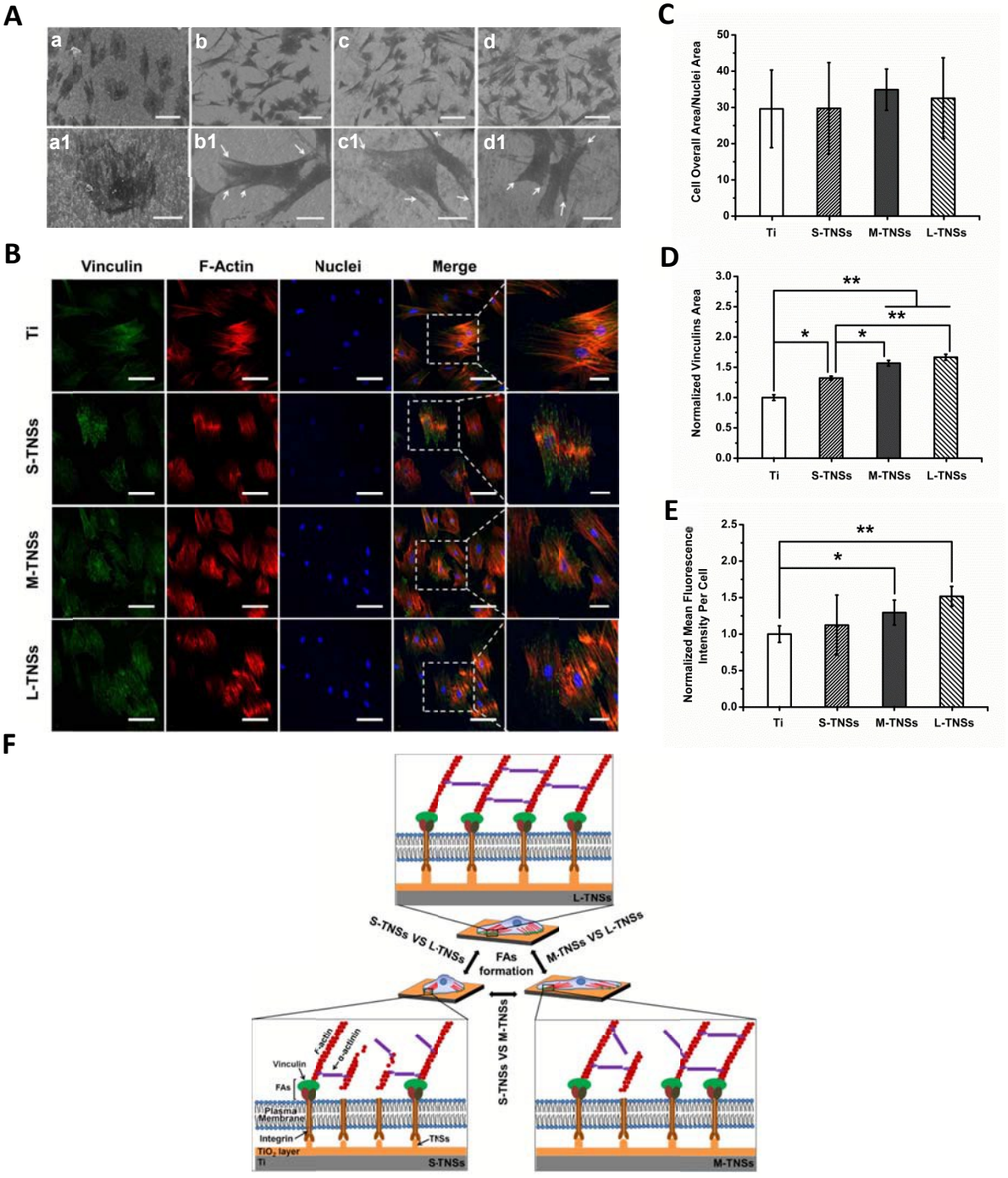

Fig. 6 (A) Representative SEM images of MSCs cultured on the different substrates: Ti (a & a1), S-TNSs (b & b1), M-TNSs (c & c1), L-TNSs (d & d1) (scale bar, 100 μm for a, b, c and d, 30 μm for a1, b1, c1 and d1, respectively); (B) Representative fluorescence images of MSCs adhered to different substrates. Cells were stained with anti-vinculin (green) for vinculins, rhodamine phalloidin (red) for actin filaments (F-actin; cytoskeleton), Hoechst 33258 (blue) for cell nuclei. The dash frames in the merged images were enlarged and shown in the right side correspondingly (scale bar, 50 μm for original images and 20 μm for enlarged images). Quantitative analysis of (C) cell spreading areas and (D) cell vinculins areas on different substrates; (E) Fluorescence intensity analysis of vinculins in cells grown onto different substrates; and (F) Schematics showing the potential mechanism of topography-induced cell FAs formation.

nanosheets adsorbed more protein (Fig. 5) and thus provided more bioactive sites for sensing MSCs, which promoting more FAs formation and then enhancing the MSCs adhesion.

Cell proliferation

To evaluate the proliferation of MSCs cultured onto different Ti substrates, FDA staining and MTT assay were performed in this study. FDA staining is a straightforward and low-cost method to qualitatively and visually evaluate cell viability. Fluorescein diacetate (FDA), a non-fluorescent hydrophobic fluorescein derivative, can be reasonably easy to penetrate into cell membranes. When the diacetate group was hydrolyzed by intracellular esterases, extremely strong green fluorescein would be generated. More importantly, the fluorescein molecules only accumulate in cells that possess intact membranes. Therefore, the green fluorescence expression indirectly reflects the numbers of viable cells.[36] Fig. 7 A shows the FDA staining of MSCs adhered to different Ti substrates after incubation for 1, 4 and 7 days, respectively. After seeding for 1 day, MSCs well distributed onto different substrates and TCPS. After culture for 4 days, more MSCs were found on M-TNSs and L-TNSs substrates when comparing with that of native Ti substrates. After further incubation for 7 days, cells almost completely covered the surface of M-TNSs and L-TNSs substrates in an aggregation form. However, relatively low density of cells was found on Ti and S-TNSs substrates.

Furthermore, we quantitatively evaluated cell proliferation with MTT method. Fig. 7 B shows the viability of MSCs cultured on different Ti substrates and TCPS after culture for 7 and 14 days, respectively. After culture for 7 days, MSCs grown onto M-TNSs substrates displayed statistically higher ($p<0.05$) cell viability than that of native Ti substrates. However, no significant difference in cell viability was observed between any others groups. After culture for 14 days, MSCs seeded onto M-TNSs and L-TNSs substrates showed significantly higher ($p<0.01$, or $p<0.05$) cell viability than that of native Ti substrates. Nevertheless, there was still no statistical difference in cell viability between M-TNSs and L-TNSs substrates.

In short, Ti substrates with sub-micrometer nanosheets-pores topography had prominent effect on cell viability. For the substrates with larger-size nanosheets, MSCs could not only be provided more adhesion sites, but search for more protein aggregates, and as a result, MSCs grown onto M-TNSs and L-TNSs substrates had higher cell viability than that of S-TNSs and pure Ti substrates. In addition, it was related to the fact that M-TNSs and L-TNSs substrates were more beneficial for retaining the bioactivity of the absorbed protein.[52]

Osteogenic differentiation of MSCs with or without osteoinductive medium

In this section, we investigated the effects of sub-micrometer topographical Ti substrates on MSCs osteogenic differentiation with or without osteoinductive medium (OM). Normal medium (NM) is a maintenance medium that has no capacity for inducing the osteogenic differentiation of MSCs.[33] Thus, by using this medium, we could directly investigate how the sub-micrometer nanosheets-pores topography of Ti substrates affects the osteogenic differentiation of MSCs. On the other hand, to investigate

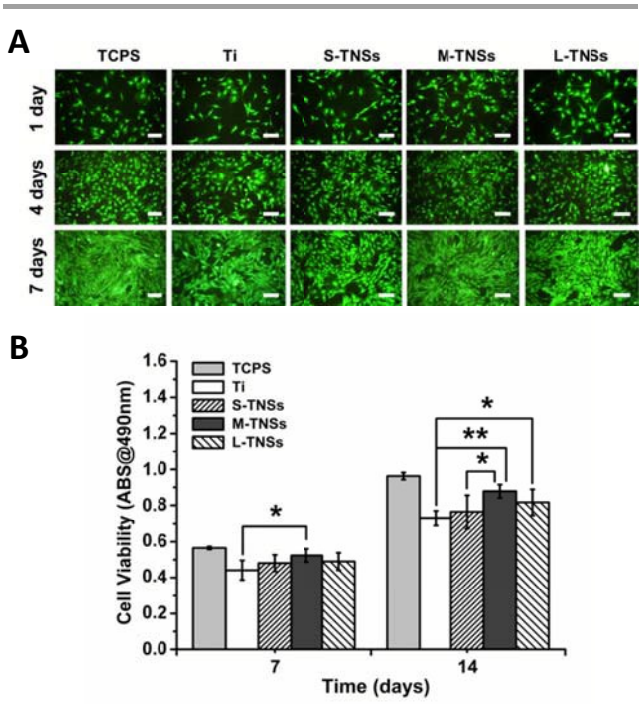

Fig. 7 Cell proliferation assays: (A) Representative fluorescence images of MSCs cultured onto different substrates (scale bar, 200 μm); and (B) MTT assay for MSCs proliferation on different substrates. Error bars represent means ± SD for n=5, *p<0.05, **p<0.01.

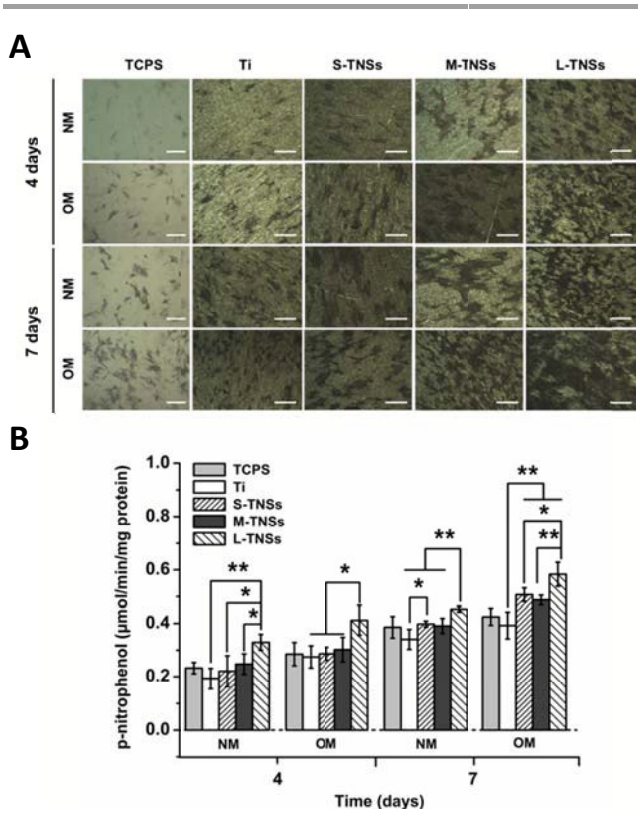

Fig. 8 ALP activity assay: (A) ALP staining of MSCs cultured onto different substrates and TCPS with normal medium (NM) and osteoinductive medium (OM) for 4 and 7 days (scale bar, 1 mm); and (B) ALP activity of MSCs adhered to different substrates for 4 and 7 days. Error bars represent means ± SD for n=5, *p<0.05, **p<0.01.

osteogenic differentiation of MSCs with OM, the cells were incubated on the first day with NM and OM for the next incubation period. The OM contains bioactive molecules including β-glycerophosphate, dexamethasone, and L-ascorbic acid. ALP staining, Alizarin Red Staining (ARS), qRT-PCR and western blot of osteogenic markers were used to evaluate osteogenic differentiation of MSCs grown onto different Ti substrates.

Amongst the major osteogenic hallmarks, the ALP expression is a key event occurring at the early stage of osteogenic differentiation of MSCs towards an osteoblast phenotype. Fig. 8 A shows the ALP staining of MSCs cultured on different Ti substrates and TCPS with NM or OM for 4 and 7 days, respectively. Under non-osteogensis inducing condition (with NM), the ALP expression of MSCs grown onto all substrates occurs after culture for 4 days and prominently increases after incubation for 7 days. Under osteogensis inducing condition (with OM), the ALP production of MSCs cultured onto different substrates was more extensive in comparison to those corresponding groups culturing with NM (Fig. 8 A). It is interesting to note that MSCs grown onto L-TNSs substrates produce more ALP than those of others substrates under both conditions.

Quantitative ALP activity assay was also performed (Fig. 8 B). Under non-osteogensis inducing condition (with NM), the ALP activity of MSCs grown onto L-TNSs substrates was statistically higher ($p<0.01$) than those of others substrates after culture for 4 and 7 days. No significant difference in ALP activity was found among native Ti, S-TNSs and M-TNSs substrates. Under osteogensis inducing condition (with OM), the ALP activity of MSCs grown onto L-TNSs substrates displayed was statistically higher ($p<005$ or $p<0.01$) than those of others substrates after culture for 4 and 7 days, respectively. The results suggest that the treated Ti substrates (in particular of L-TNSs) positively promoted the osteogenic differentiation of MSCs at an early stage.

Moreover, ARS was performed after MSCs growing onto different substrates under both conditions (NM or OM) for 21 days (Fig. 9 A). The ARS method is generally used to evaluate extracellular calcium deposition that is considered as an indicator of osteogenic differentiation of MSCs at late stage.[55] Under non-osteogensis inducing condition (with NM), obvious calcium nodules from MSCs adhered to M-TNSs and L-TNSs substrates were

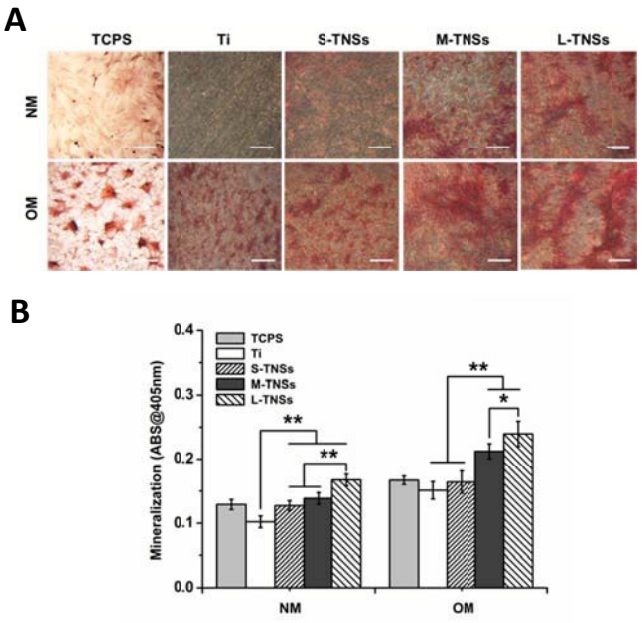

Fig. 9 ECM mineralization of MSCs cultured onto different substrates with normal medium (NM) and osteoinductive medium (OM) for 3 weeks. (A) Representative images cells stained with Alizarin Red S (scale bar, 1 mm); and (B) Quantification of cell mineralization onto different substrates (ABS means absorbance). Error bars represent means ± SD for n=5, *p<0.05, **p<0.01.

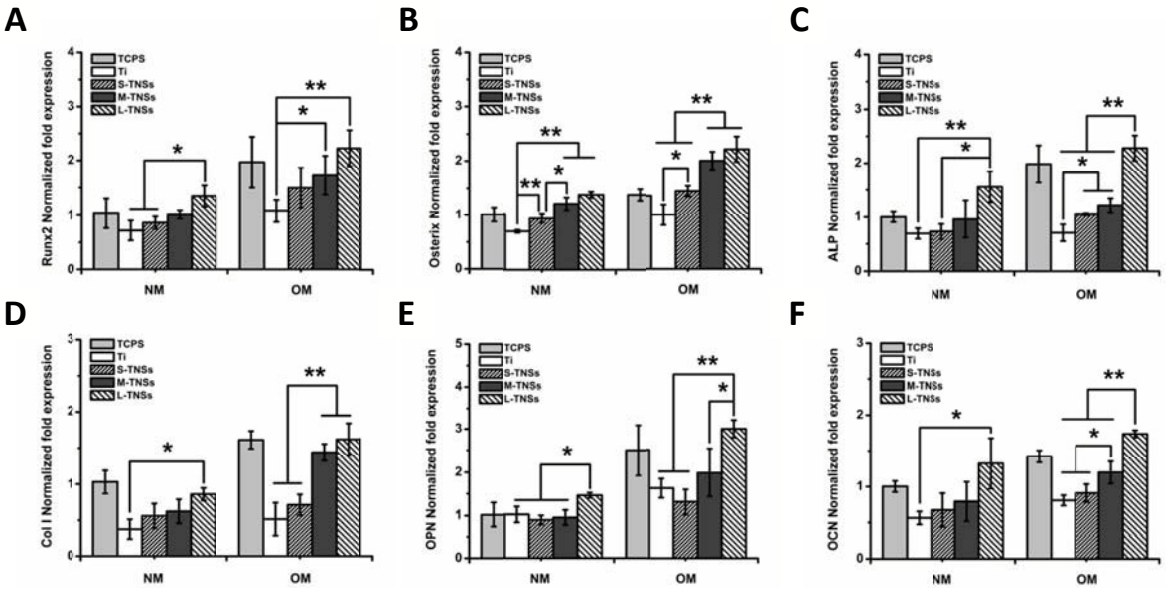

Fig. 10 Relative mRNA expression of bone formation related genes: (A) Runx2, (B) Osterix, (C) ALP, (D) Col I, (E) OPN, and (F) OCN, respectively. The MSCs were cultured on different substrates samples with normal medium (NM) and osteoinductive medium (OM) for 2 weeks. The value was normalized to β-actin. Error bars represent mean ± SD for n=4, *p<0.05, **p<0.01.

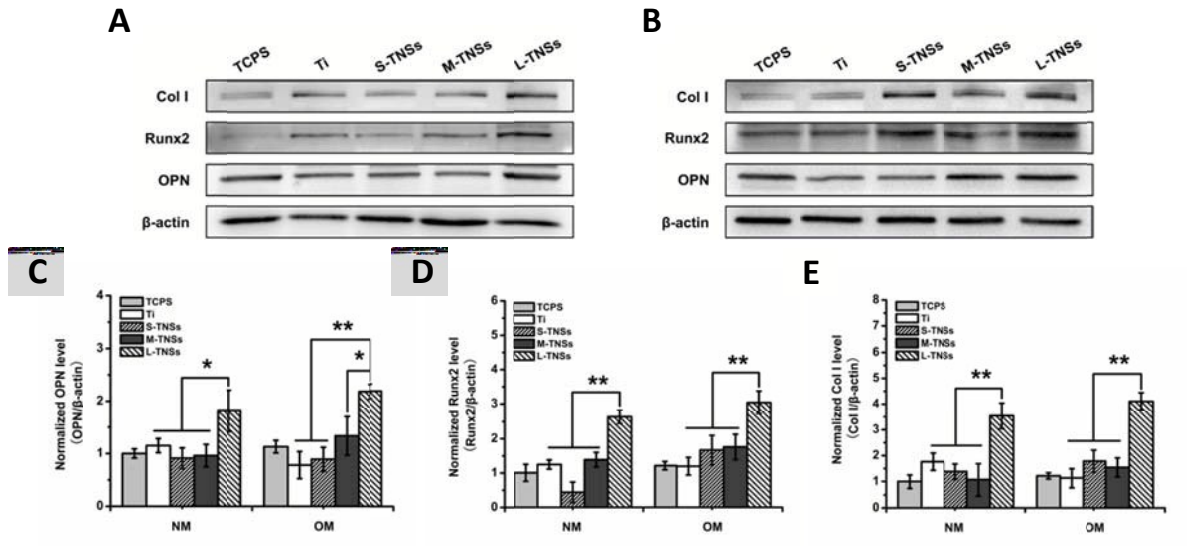

Fig. 11 Western blot assay of Runx2, Col I and OPN after 2 weeks culture on different substrates in (A) normal medium (NM) and (B) osteoinductive medium (OM). (C), (D) and (E) Quantitative western blot data showing these proteins expression levels of different substrates. Results of different substrates were normalized to that of the TCPS. Error bars represent means ± SD for n=3, *p<0.05, **p<0.01.

observed, in comparison to trivia calcium nodules formation onto Ti and S-TNSs substrates. Under osteogensis inducing condition (with OM), there was extensive calcium nodules formation on all substrates, in particular of L-TNSs sample (Fig. 9 A).

The biomineralization of MSCs was also quantitatively measured (Fig. 9 B). Under non-osteogensis inducing condition (with NM), MSCs cultured onto L-TNSs substrates displayed significantly higher (p<0.01) mineralization than those of Ti, S-TNSs and M-TNSs substrates, which was consistent with ALP staining observation (Fig. 9 A). Thus, both qualitative and quantitative characterizations of calcium deposition of MSCs demonstrate that sub-micrometer nanosheets-pores topography of Ti substrates enhanced the biomineralization of MSCs. Under osteogensis inducing condition (with OM), MSCs grown onto L-TNSs substrates displayed higher (p<0.05 or p<0.01) mineralization than those of the others substrates (Fig. 9 B).

We quantitatively characterized the gene expression of osteogenic markers (Runx2, Osterix, ALP, Col I, OPN, and OCN) under both conditions (NM or OM) by qRT-PCR after culture for 14 days. As crucial transcription factors in the osteogenic differentiation of MSCs, Runx2 and Osterix could regulate the transcription of downstream osteogenic genes (ALP, Col I, OCN, OPN, etc.).[27,56-58] Herein, the expression level of Runx2 in the group of L-TNSs was significantly up-regulated (p<0.05 or p<0.01) comparing with those of Ti and S-TNSs groups (Fig. 10 A). Similar trend was also observed for Osterix expression (Fig. 10 B). Although ALP is an extremely critical marker of osteogenic differentiation of MSCs at early stage, it could be acted as a symbol to reflect the lasting effect of material topography on osteogenic differentiation of MSCs at the middle and late stages.[59] As shown in Fig. 10 C, the ALP expression in L-TNSs group was significantly up-regulated (p<0.05 or p<0.01) when comparing others groups. For Col I, a mature marker of osteogenic differentiation and one of the most abundant ECM proteins in bone tissue,[29] the expression level between the L-TNSs and Ti displayed statistical difference (p<0.05 or p<0.01) (Fig. 10 D). Subsequently, we evaluated the gene expressions of osteogenic-related proteins (OCN and OPN) of MSCs growing onto different Ti substrates. OCN is the most abundant non-collagenous protein in nature bone and one of the markers reflecting osteogenic differentiation and bone formation.[32,60] OPN is a structural protein and plays a vital role in bone remodeling.[61] These two proteins could maintain bone-like nodules formation for the further development of complicated three-dimensional mineralized structures. As illustrated in Fig. 10 E, the OPN expression level of MSCs between L-TNSs and others Ti substrates displayed statistical difference (p<0.05 or p<0.01). As for OCN expression, a similar trend to OPN was observed (Fig. 10 F). Thus, we could find that Runx2, Osterix, ALP, Col I, OPN and OCN genes expressions were sensitive to the sub-micrometer nanosheets-pores topographies of Ti substrates, and L-TNSs substrates had the highest genes expression levels among all groups (Fig. 10). Also, we investigated the protein levels of Runx2, Col I and OPN under NM and OM conditions by Western-blot assay after culture for 14 days, since the three proteins are critical markers in the osteogenic differentiation of MSCs. As shown in Fig. 11, whether under NM or OM conditions, the protein levels of Runx2, Col I and OPN for the cells cultured onto the L-TNSs substrates were significantly higher (p<0.05 or p<0.01) than those for the cells adhered to the others substrates. The results were almost entirely consistent with that of qRT-PCR assay (Fig. 10). In short, qualitative and/or quantitative assays of ALP activity, biomineralization, genes/proteins expressions of osteogenic markers proved that the sub-micrometer nanosheets-pores topography of Ti substrates (especially the L-TNSs), could enhance osteogenic differentiation of MSCs.

Taken together, we confirmed our hypothesis that the sub-micrometer nanosheets-pores topography of Ti substrates could improve cell adhesion and osteogenic differentiation of MSCs. The presence of the sub-micrometer nanosheets-pores topography triggers a series of biological events of MSCs. The fates of MSCs were highly regulated by their surviving microenvironment. On the one hand, MSCs actively adjusted the FAs in response to signals deriving from their ECM environment, such as surface chemistry,

topographical structures, and physical forces *etc.*[21,22,53,54] Some other surface modified substrates by using MAO, ECO, *etc.* techniques had been reported to regulate the fate of MSCs.[10,11,49] However, some of them were based on the increasing surface roughness and area, which was just one of causes of FAs organization and a series of subsequent cell behaviors. No matter what changes of surface characteristics occur, MSCs would firstly sense the changes through integrin /FAs /actin filaments, and then accurately respond to the changes. Once MSCs come into contacting with a substrate, this sense-response pattern would accompany with the whole life of MSCs. Thus, we could easily observe the comprehensive effects from surface modified substrates on cell functions by understanding the pivotal roles of FAs. In this study, the sub-micrometer nanosheets-pores topography of Ti substrates promoted FAs formation of MSCs, which were clearly reflected by vinculin expression and normalized vinculin areas (Fig. 6, B, D & E). The enhanced FAs of MSCs grown on the sub-micrometer nanosheets-pores topographical surfaces would then contribute to the osteogenic differentiation of MSCs. On the other hand, growing onto Ti substrates with large nanosheets structures (L-TNSs), MSCs are more difficult to interact with protein aggregates, and as a result, they are guided to differentiate into osteoblasts,[10] along with time-dependent osteogenic differentiation events, *i.e.*, Runx2/ALP transcripts upregulation, bone-related matrix protein expression (OCN, OPN, *etc.*), and matrix mineralization (Fig. 7). Consequently, the reduced cell activity and the enhanced osteogensis ability appeared simultaneously.[10] While under OM condition, bioactive molecules and substrate topography synergistically contributed to the osteogenic differentiation of MSCs.

Conclusions

In summary, we successfully fabricated sub-micrometer topography composed of nanosheets-pores structures on pure titanium surfaces via vapor alkaline treatment along with ion exchange and calcination treatment, which was revealed by combined techniques of SEM, AFM XPS, XRD and contact angle measurement, respectively. The sub-micrometer nanosheets-pores topographical titanium substrates improved the adhesion, proliferation and differentiation of MSCs on cellular level. Moreover, sub-micrometer topographical Ti substrates, especially the L-TNSs, up-regulated the expressions of bone formation related genes/proteins (Runx2, Osterix, ALP, Col I, OPN and OCN), and thus accelerating the differentiation of MSCs into osteoblasts on molecular level. The study affords an alternative for the fabrication of high quality titanium-based implants.

Acknowledgements

The work was financially supported by National Natural Science Foundation of China (51173216 and 31170923), Natural Science Foundation of Chongqing Municipal Government (CSTC2013kjrc-ljrcpy0004, CSTC2013jjB50004), National Key Technology R&D Program of the Ministry of Science and Technology (2012BAI18B04) and Fundamental Research Funds for the Central Universities (CQDXWL-2013-Z002).

Notes and References

1 A. Higuchi, Q.D. Ling, Y.A. Ko, Y. Chang, A. Umezawa, *Chem. Rev.*, 2011, **111**, 3021.
2 F. Osakada, H. Ikeda, M. Mandai, T. Wataya, K. Watanabe, N. Yoshimura, A. Akaike, Y. Sasai, M. Takahashi, *Nat. Biotechnol.*, 2008, **26**, 215.
3 M.F. Pittenger, A.M. Mackay, S.C. Beck, R.K. Jaiswal, R. Douglas, J.D. Mosca, A. Akaike, Y. Sasai, M. Takahashi, *Science*, 1999, **284**, 143.
4 A.J. Wagers, I.L. Weissman, *Cell*, 2004, **116**, 639.
5 K.A. Moore, I.R. Lemischka, *Science*, 2006, **311**, 1880.
6 D. Zhang, K.A. Kilian, *Biomaterials*, 2013, **34**, 3962.
7 M.J. Dalby, N. Gadegaard, R. Tare, A. Andar, M.O. Riehle, P. Herzyk, C.D.W. Wilkinson, R.O.C. Oreff, *Nat. Mater.*, 2007, **6**, 997.
8 E. Cukierman, R. Pankov, D.R. Stevens, K.M. Yamada, *Science*, 2001, **294**, 1708.
9 B. Trappmann, J.E. Gautrot, J.T. Connelly, D.G. Strange, Y. Li, M.L. Oyen, M.A.C. Stuart, H. Boehm, B.J. Li, V. Vogel, J.P. Spatz, F.M. Watt, W.T.S Huck, *Nat. Mater.*, 2012, **11**, 642.
10 S. Oh, K.S. Brammer, Y.S. Li, D. Teng, A.J. Engler, S. Chien, S. Jin, *Proc. Natl. Acad. Sci. U. S. A.*, 2009, **106**, 2130.
11 J. Park, S. Bauer, K. von der Mark, P. Schmuki, *Nano Lett.*, 2007, **7**, 1686.
12 W.J. Zhang, Z.H. Li, Q.F. Huang, L. Xu, J.H. Li, Y.Q. Jin, X.Y. Liu, X.Q., *Int. J. Nanomed.*, 2013, **8**, 257.
13 R.K. Das, O.F. Zouani, C. Labrugere, R. Oda, M.C. Durrieu, *ACS NANO*, 2013, **7**, 3351.
14 S. Watari, K. Hayashi, J.A. Wood, P. Russell, P.F. Nealey, C.J. Murphy, D.C. Genetos, *Biomaterials*, 2012, **33**, 128.
15 K.C. Popat, K.I. Chatvanichkul, G.L. Barnes, T.J. Latempa Jr., C.A. Grimes, T.A. Desai, *J. Biomed. Mater. Res. A*, 2006, **6**, 955.
16 L. Prodanov, E. Lamers, M. Domanski, R. Luttge, J.A. Jansen, X.F. Walboomers, *Biomaterials*, 2013, **34**, 2920.
17 M. Long, H.J. Rack, *Biomaterials*,1998, **19**, 1621.
18 R.M. Pillar, J.M. Lee, C. Maniatopoulos, *Clin. Orthop. Rel. Res.*, 1986, **208**, 108.
19 S.M. Sporer, W.G. Paprosky, *Orthop. Clin. North Am.*, 2005, **36**, 105.
20 M.M. Stevens, J.H. George, *Science*, 2005, **318**, 1135.
21 E.K. Yim, E.M. Darling, K. Kulangara, F. Guilak, K.W. Leong, *Biomaterials*, 2010, **31**, 1299.
22 C.H. Seo, K. Furukawa, K. Montagne, H. Jeong, T. Ushida, *Biomaterials*, 2011, **32**, 9568.
23 P.R. Liu, H.M. Zhang, H.W. Liu, Y. Wang, X.D. Yao, G.S. Zhu, S.Q. Zhang, H.J. Zhao, *J. Am. Chem. Soc.*, 2011, **133**, 19032.
24 M. Takemoto, S. Fujibayashi, M. Neo, J. Suzuki, T. Matsushita, T. Kokubo, T. Nakamura, *Biomaterials*, 2006, **27**, 2682.
25 S. Fujibayashi, T. Nakamura, S. Nishiguchi, J. Tamura, M. Uchida, H.M. Kim, T. Kokubo, *J. Biomed. Mater. Res.*, 2001, **56**, 562.
26 J.H. Li, W.J. Zhang, Y.Q. Qiao, H.Q. Zhu, X.Q. Jiang, X.Y. Liu, C.X. Ding, *J. Mater. Chem. B*, 2014, **2**, 283.

27 X.K. Shen, Y. Hu, G.Q. Xu, W.Z. Chen, K. Xu, Q.C. Ran, P.P. Ma, Y.R. Zhang, J.H. Li, K.Y. Cai, *ACS Appl. Mater. Interfaces*, 2014, **6**, 16426.
28 I. Pountos, D. Corscadden, P. Emery, P.V. Giannoudis, *Injury*, 2007, **38**, S23.
29 M.J. Kim, B. Lee, K. Yang, J. Park, S. Jeon, S.H. Um, D.I. Kim, S.G. Im, S.W. Cho, *Biomaterials*, 2013, **34**, 7236.
30 K.Y. Cai, K.D. Yao, S.B. Lin, Z.M. Yang. *J Biomater Sci Polym Edn*, 2001,**12**, 1303.
31 A.K. Gaharwar, S.M. Mihaila, A. Swami, A. Patel, S. Sant, R.L. Reis, A.P. Marques, M.E. Gomes, A. Khademhosseini, *Adv. Mater.*, 2013, **5**, 3329.
32 W.H. Yang, X.F. Xi, Y. Si, S. Huang, J.F. Wang, K.Y. Cai, *Acta Biomater.*, 2014, **10**, 4525.
33 K.Y. Cai, J. Bossert, K.D. Jandt, *Colloid. Surface. B*, 2006, **49**, 136.
34 K.Y. Cai, Y. Hu, K.D. Jandt. *J Mater Sci Mater Med* 2008, **19**, 499.
35 K.Y. Cai, M. Lai, W.H. Yang, R. Hu, R.L. Xin, Q. Liu, K.L.P. Sung, *Acta Biomater.*, 2010, **6**, 2314.
36 F. Liao, Y.Y. Chen, Z.B. Li, Y.N. Wang, B. Shi, Z.C. Gong, X.R. Cheng, *J. Mater. Sci. Mater. Med.*, 2010, **21**, 489.
37 M. Lai, K.Y. Cai, L. Zhao, X.Y. Chen, Y.H. Hou, Z.X. Yang, *Biomacromolecules*, 2011, **12**, 1097.
38 L.Z. Zhao, L. Liu, Z.F. Wu, Y.M. Zhang, P.K. Chu, *Biomaterials*, **33**, 2629.
39 K.Y. Cai, K.D. Yao, X. Hou, Y.Q. Wang, Y.J. Hou, Z.M. Yang, X.Q. Li, H.Q. Xie, *J. Biomed. Mater. Res.*, 2002, **62**, 283.
40 J. Park, S. Bauer, K.A. Schlegel, F.W. Neukam, K. von der Mark, P. Schmuki, *Small*, 2009, **5**, 666.
41 S. Yamaguchi, S. Nath, T. Matsushita, T. Kokubo, *Acta Biomater.*, 2014, **10**, 2282.
42 M. Uchida, H.M. Kim, T. Kokubo, S. Fujibayashi, T. Nakamura, *J. Biomed. Mater. Res.*, 2002, **63**, 522.
43 Y. Han, D. Chen, J. Sun, Y. Zhang, *Acta Biomater.*, 2008, **4**, 1518.
44 B. Feng, J.Y. Chen, S.K. Qi, L.J. He, Z. Zhao, X.D. Zhang, *J. Mater. Sci.: Mater M.*, 2002, **13**, 457.
45 H.K. Jang, S.W. Whangbo, H.B. Kim, K.Y. Im, Y.S. Lee, I.W. Lyo, C.N. Whang, G. Kim, H.S. Lee, J.M. Lee, *J. Vac. Sci. Technol. A*, 2000, **18**, 917.
46 C.C. Ting, S.Y. Chen, D.M. Liu, *J. Appl. Phys.*, 2000, **88**, 4628.
47 S.O. Kang, H.S. Jang, Y.I. Kim, K.B. Kim, M.J. Jung, *Mater. Lett.*, 2007, **61**, 473.
48 E. Hosono, H. Matsuda, I. Honma, M. Ichihara, H.S. Zhou, *Langmuir*, 2007, **23**, 7447.
49 K.M. Wu, W. Song, L.Z. Zhao, M.Y. Liu, J. Yan, M. Ø. Andersen, J. Kjems, S. Gao, Y.M. Zhang, *ACS Appl. Mater. Interfaces*, 2013, **5**, 2733.
50 I. Lynch, *Physica A*, 2007, **373**, 511.
51 M. Han, A. Sethuraman, R.S. Kane, G. Belfort, *Langmuir*, 2003, **19**, 9868.
52 J. Lu, C. Yao, L. Yang, T.J. Webster, *Tissue Eng. Part A*, 2012, **18**, 1389.
53 K. Hu, L. Ji, K.T. Applegate, G. Danuser, C.M. Waterman-Storer, *Science*, 2007, **315**, 111.
54 M.A. Wozniak, K. Modzelewska, L. Kwong, P.J. Keely, *Biochimica et Biophysica Acta*, 2004, **1692**, 103.
55 H.C. Anderson, *Lab. Invest.*, 1989, **60**,320.
56 X.Y. Ma, Y.F. Feng, Z.S. Ma, X. Li, J. Wang, L. Wang, W. Lei, *Biomaterials*, 2014, **35**, 7259.
57 D. Xu, L. Xu, C. Zhou, W.Y. Lee, T. Wu, L. Cui, G. Li, *Int. J. Biochem. Cell Biol.*, 2014, **51**, 1.
58 Y. Hu, K.Y. Cai, Z. Luo, Y. Zhang, L.Q. Li, M. Lai, Y.H. Hou, Y.R. Huang, J.H. Li, X.W. Ding, B. Zhang, K.L.P. Sung, *Biomaterials*, **33**, 3515.
59 M.T. Harris, D.L. Butler, G.P. Boivin, J.B. Florer, E.J. Schantz, R.J. Wenstrup, *J. Orthop. Res.*, 2004, **22**, 998.
60 P. Ducy, C. Desbois, B. Boyce, G. Pinero, B. Story, C. Dunstan, E. Smith, J. Bonadio, S. Goldstein, C. Gundberg, A. Bradley, G. Karsenty, *Nature*, 1996, **382**, 448.
61 W.T. Butler, *Tissue Res.*, 1989, **23**, 123.

Entry for the Table of Contents

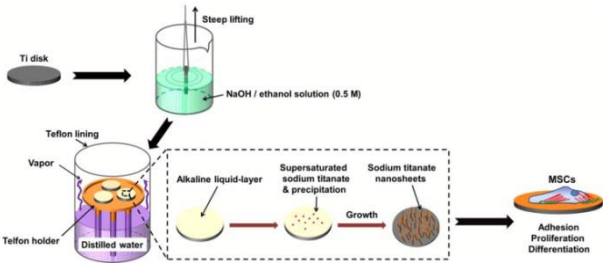

Sub-micrometer nanosheets-pores topographic titanium substrates are fabricated with distinct effect on the adhesion and osteogenic differentiation of MSCs *in vitro*.